9072 *Inorg. Chem.* **2009**, *48*, 9072–9076
DOI: 10.1021/ic901084s

Inorganic Chemistry
Article

Template-Free Hydrothermal Synthesis and Photocatalytic Performances of Novel Bi_2SiO_5 Nanosheets

Ruigen Chen,[†] Jinhong Bi,[†] Ling Wu,[*,†,‡] Wanjun Wang,[†] Zhaohui Li,[†] and Xianzhi Fu[*,†]

[†]*State Key Laboratory Breeding Base of Photocatalysis, Research Institute of Photocatalysis, Fuzhou University, Fuzhou 350002, P. R. China, and* [‡]*State Key Laboratory of Structural Chemistry, Fujian Institute of Research on the Structure of Matter, Chinese Academy of Sciences, Fuzhou, 350002, P. R. China*

Received December 3, 2008

Orthorhombic Bi_2SiO_5 nanosheets with thicknesses of 10−20 nm were first synthesized by a template-free hydrothermal synthesis process using $Bi(NO_3)_3$ and different Si sources as raw materials. The as-prepared samples were characterized by X-ray diffraction, Brunauer−Emmett−Teller (BET) surface area analysis, UV−vis diffuse reflectance spectroscopy, scanning electron microscopy, high-resolution transmission electron microscopy, and a photoluminescence technique with terephthalic acid. The results showed that different precursors led to samples with different morphologies, particle sizes, and BET surface areas. As a novel photocatalyst, the photocatalytic performances of Bi_2SiO_5 samples were evaluated by the photocatalytic degradation of salicylic acid and gaseous benzene. The results revealed that the sample obtained from Na_2SiO_3 as a precursor exhibited higher activity than that from $(C_2H_5O)_4Si$ due to its biscuit-like morphology, a smaller particle size, and a higher BET surface areas.

1. Introduction

Aurivillius-phase Bi_2SiO_5 (BSO) crystallizes in the orthorhombic system with a space group of $Cmc2_1$. Its two-dimensional structure is built up from an intergrowth of $(SiO_3)^{2-}$ pyroxene file layers inserted between $(Bi_2O_2)^{2+}$ layers. The $(Bi_2O_2)^{2+}$ layers are formed of slightly distorted squared oxygen planes. These squares are capped alternatively above and below by the bismuth atoms. Pyroxene file layers are made of corner-sharing SiO_4 tetrahedra in columns parallel to (Bi_2O_2) planes. The SiO_4 tetrahedra are slightly distorted.[1] It has been reported as a material with relatively good dielectric properties and pyroelectric and nonlinear optical effects.[2] Moreover, BSO has been applied as a promising catalyst for the oxidative coupling of methane.[3] The photocatalytic properties of BSO have not been reported, although some bismuth mixed oxide photocatalysts with similar structure, such as Bi_2WO_6,[4] Bi_2MoO_6,[5] Bi_2GeO_5,[6] and so on, have been reported. The $(Bi_2O_2)^{2+}$ layers and SiO_4 tetrahedra in the crystal structure of BSO are slightly distorted. The distorted structure of SiO_4 tetrahedra may be in favor of the separation of the photogenerated holes and electrons. Therefore, a higher degree of photocatalytic activity of the BSO is expected.[7] It would be rather valuable to evaluate the photocatalytic activity of the BSO nanostructrues.

To date, the synthetic methods for BSO have been focused on spontaneous crystallization of the overcool melted mixture of Bi_2O_3 and SiO_2 in platinum crucibles.[3] Unfortunately, some impurities such as $Bi_4Si_3O_{12}$ and $Bi_{12}SiO_{20}$ were obtained spontaneously as the stable phases because of the metastable property of BSO. Thus, successful synthetic strategies for the preparation of pure BSO nanocrystals, especially for those nanorods, nanobelts, nanosheets, and so on, are still formidable challenges. In this regard, a hydrothermal synthesis is the most appealing,[8] due to its various advantages such as a high reactivity of the reactants, facile control of the solution or interface reactions, formation

*Corresponding author e-mail: wuling@fzu.edu.cn (L.W.); xzfu@fzu.edu.cn (X.F.). Tel./Fax: 86-591-83738608.

(1) Geoges, S.; Goutenoire, F.; Lacorre, P. *J. Solid State Chem.* **2006**, *197*, 4020–4028.
(2) Koiwa, I.; Kanehara, T.; Mita, J.; Iwabuchi, T.; Osaka, T.; Ono, S.; Maeda, M. *Jpn. J. Appl. Phys.* **1996**, *35*, 4946.
(3) Voskresenkaya, E. N.; Kurteeva, L. I.; Zhereb, V. P.; Anshits, A. G. *Catal. Today* **1992**, *13*, 599.
(4) (a) Wu, L.; Bi, J.; Li, Z.; Wang, X.; Fu, X. *Catal. Today* **2008**, *131*, 15. (b) Li, Y.; Liu, J.; Huang, X.; Li, G. *Cryst. Growth Des.* **2007**, *7*, 1350. (c) Zhang, C.; Zhu, Y. *Chem. Mater.* **2005**, *17*, 3537.
(5) (a) Bi, J.; Wu, L.; Li, J.; Li, Z.; Wang, X.; Fu, X. *Acta Mater.* **2007**, *55*, 4699. (b) Zhao, X.; Qu, J.; Liu, H.; Hu, C. *Environ. Sci. Technol.* **2007**, *41*, 6802.
(6) Chen, R. G.; Bi, J. H.; Wu, L.; Li, Z. H.; Fu, X. Z. *Cryst. Growth Des.* **2009**, *9*, 1775–1779.
(7) (a) Sato, J.; Saito, N.; Nishiyama, H.; Inoue, Y. *J. Phys. Chem. B* **2001**, *105*, 6061–6063. (b) Sato, J.; Satio, N.; Nishiyama, H.; Inoue, Y. J. *J. Photochem. Photobiol., A* **2002**, *148*, 85–89. (c) Kadowaki, H.; Sato, J.; Kobayashi, H.; Satio, N.; Nishiyama, H.; Simodaira, Y.; Inoue, Y. *J. Phys. Chem. B* **2005**, *109*, 22995–23000. (d) Sato, J.; Ikarashi, K.; Kobayshi, H.; Satio, S.; Nishiyama, H.; Inoue, Y. *J. Phys. Chem. B* **2004**, *108*, 4369. (e) Hou, Y.; Wu, L.; Wang, X.; Ding, Z.; Li, Z.; Fu, X. *J. Catal.* **2007**, *250*, 12–18.
(8) (a) Lin, J.; Lin, J.; Zhu, Y. *Inorg. Chem.* **2007**, *46*, 8372. (b) Huang, J.; Wang, X.; Hou, Y.; Chen, X.; Wu, L.; Fu, X. *Environ. Sci. Technol.* **2008**, *42*, 7387. (c) Liang, J.; Peng, Q.; Wang, X.; Zheng, X.; Wang, R.; Qiu, X.; Nan, C.; Li, Y. *Inorg. Chem.* **2005**, *44*, 9405.

Published on Web 09/09/2009

of metastable and unique condensed phases, less air pollution, and low energy consumption.[9] Many kinds of materials with special morphologies such as nanosheets, nanoplates, nanorods, nanotubes, and so forth have been prepared by this synthetic approach.[10] Nonetheless, conventional hydrothermal methods for the preparation of these materials usually require removable or sacrificial templates,[11] and disadvantages related to high cost and tedious synthetic procedures may prevent them from being used in large-scale applications. Ideally, one would prefer a template-free hydrothermal synthesis process for the controlled preparation of nanostructures with special morphologies.

Here, orthorhombic BSO nanosheets were synthesized successfully by a template-free hydrothermal synthetic process. This is the fastest and first reported direct synthesis of such materials. This approach also eliminates the need for any air-sensitive, toxic, and expensive starting material. The effects of the precursor on the morphology, particle size, and Brunauer−Emmett−Teller (BET) surface area of BSO were discussed. Furthermore, the applications of BSO nanosheets in the photocatalytic decomposition of organic pollutants were also investigated for the first time.

2. Experimental Section

2.1. Synthesis. In a typical synthesis, 1.84 g of $Bi(NO_3)_3 \cdot 5H_2O$ (mmol) and 0.54 g of $Na_2SiO_3 \cdot 9H_2O$ (mmol) were added into 75 mL of deioned water. Under vigorous stirring, the pH value of the mixture was adjusted to 9 through the dripping of 10% $NH_3 \cdot H_2O$. After stirring for 20 min, the mixture was transferred into a Teflon-lined autoclave with a capacity of 100 mL. Then, the autoclave was sealed, heated under autogenous pressure at 180 °C for 48 h, and then allowed to cool to room temperature naturally. The solid products were collected and washed with distilled water and absolute ethanol several times and then dried at 80 °C for 8 h. A white Bi_2SiO_5 powder sample was obtained with a high yield of ∼90% and is denoted as BSO(2). The other sample was prepared by the similar procedure, except for different Si sources, instead by tetraethyl orthosilicate ($(C_2H_5O)_4Si$). The obtained powder sample was denoted as BSO(1).

2.2. Characterization. The as-prepared samples were characterized by powder X-ray diffraction (XRD) on a Bruker D8 Advance X-ray diffractometer at 40 kV and 40 mA with Ni-filtered Cu Kα radiation. Data were recorded at a scan rate of 0.02° 2θ s^{-1} in the 2θ range 10−70°. BET surface area was measured by using ASAP2020 M from Micromeritics Instrument Corporation. The general morphology of the samples was examined using scanning electron microscopy (SEM) on a JEOL JSM 6700F instrument operated at 20 kV and equipped with an energy-dispersive X-ray analyzer (Phoenix). The morphology was also further investigated using transmission electron microscopy (TEM) and high-resolution TEM (HRTEM) using a JEOL JEM 2010F microscope working at 200 kV. UV−vis diffuse reflectance spectra (UV−vis DRS) of the samples were obtained for the dry-pressed disk sample using a UV−visible spectrophotometer (Lambda-900, Perkin−Elmer). $BaSO_4$ was used as a reflectance standard. The generation of

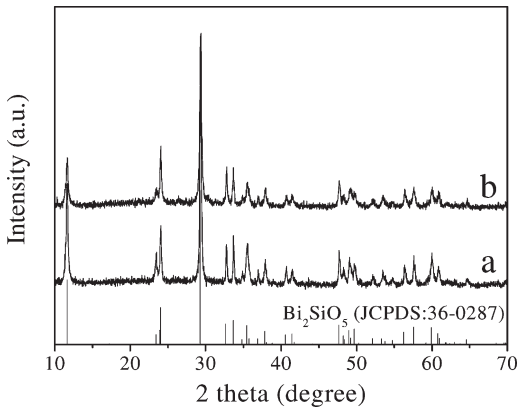

Figure 1. XRD patterns of BSO samples: (a) BSO(1) and (b) BSO(2).

•OH radicals was investigated through the method of photoluminescence with terephthalic acid. The •OH-trapping photoluminescence spectra were surveyed using an Edinburgh FL/FS900 spectrophotometer.

2.3. Photocatalytic Activity Measurements. Photocatalytic reactions of salicylic acid were performed in a quartz tube with a 4 cm inner diameter and a 17.7 cm length. Three 4 W UV lamps with a wavelength centered at 254 nm (Philips, TUV4 W/G4 T5) were used as an illuminating source. A total of 100 mg of powdered photocatalyst was suspended in 150 mL of salicylic acid aqueous solution (2.5×10^{-4} mol/L). Vigorous stirring and oxygen bubbling (20 mL/min) were set up during the photocatalytic process. Before irradiation, the suspension was stirred in the dark for 2 h to ensure the adsorption/desorption equilibrium. A 3 mL aliquot was taken and centrifuged at 20 min intervals during the experiment. The resulting clear liquor was analyzed on a Varian Cary-50 UV−vis−NIR spectrophotometer. The percentage of degradation was reported as C/C_0, where C was the absorption of salicylic acid at each irradiated time interval of the main peak of the absorption spectrum at a wavelength of 297 nm and C_0 was the absorption of the starting concentration when adsorption/desorption equilibrium was achieved.

To further evaluate the photocatalytic activities of Bi_2SiO_5 catalysts, the photocatalytic decomposition of gaseous benzene was also conducted with a fixed-bed tubular quartz reactor operated in a single-pass mode. The catalyst (0.3 g) was loaded in the reactor surrounded by four 4 W UV lamps with a wavelength centered at 254 nm (Philips, TUV 4W/G4 T5). Benzene diluted in a pure oxygen stream was used to afford a reactant stream. The initial concentrations of benzene and carbon dioxide in the stream were determined to be 300 ppm and 0 ppm, respectively. The flow rate of the reactant stream was kept at 20 mL/min. Simultaneous determination of C_6H_6 and CO_2 concentrations was performed with an online gas chromatograph (HP6890) equipped with a flame ionization detector, a thermal conductivity detector, and a Porapak R column. The reaction temperature was controlled at 29 ± 1 °C with an air-cooling system.

3. Results and Discussion

3.1. XRD Analyses and BET Surface Areas of the Bi_2SiO_5 Products. Figure 1 shows the XRD patterns of the products obtained by different Si precursors. All of the observed peaks of the pattern can be indexed to a pure orthorhombic Bi_2SiO_5 phase (JCPDS 36−0287). No other peaks are found, suggesting the high purity and crystallinity of the samples. The average crystallite sizes calculated via the Scherrer equation from the (311) peak (2θ = 29.2°) are 33.9 nm for BSO(1) and 28.8 nm for

(9) Feng, S.; Xu, R. *Acc. Chem. Res.* **2001**, *34*, 239.
(10) (a) Charles Cao, Y. *J. Am. Chem. Soc.* **2004**, *126*, 7456. (b) Ren, G.; Lin, Z.; Gilbert, B.; Zhang, J.; Huang, F.; Liang, J. *Chem. Mater.* **2008**, *20*, 2438. (c) Chen, X.; Sun, X. M.; Li, Y. D. *Inorg. Chem.* **2002**, 4524–4530. (d) Yang, J.; Lin, C. K.; Wang, Z. L.; Lin, J. *Inorg. Chem.* **2006**, *45*, 8973–8979. (e) Ke, D. N.; Peng, T. Y.; Ma, L.; Cai, P.; Dai, K. *Inorg. Chem.* **2009**, *48*, 4685–4691.
(11) (a) Ah, C. S.; Yun, Y. J.; Park, H. J.; Kim, W. J.; Ha, D. H.; Yun, W. S. *Chem. Mater.* **2005**, *17*, 5558. (b) Liu, Y.; Xu, H.; Qian, Y. *Cryst. Growth Des.* **2006**, *6*, 1304.

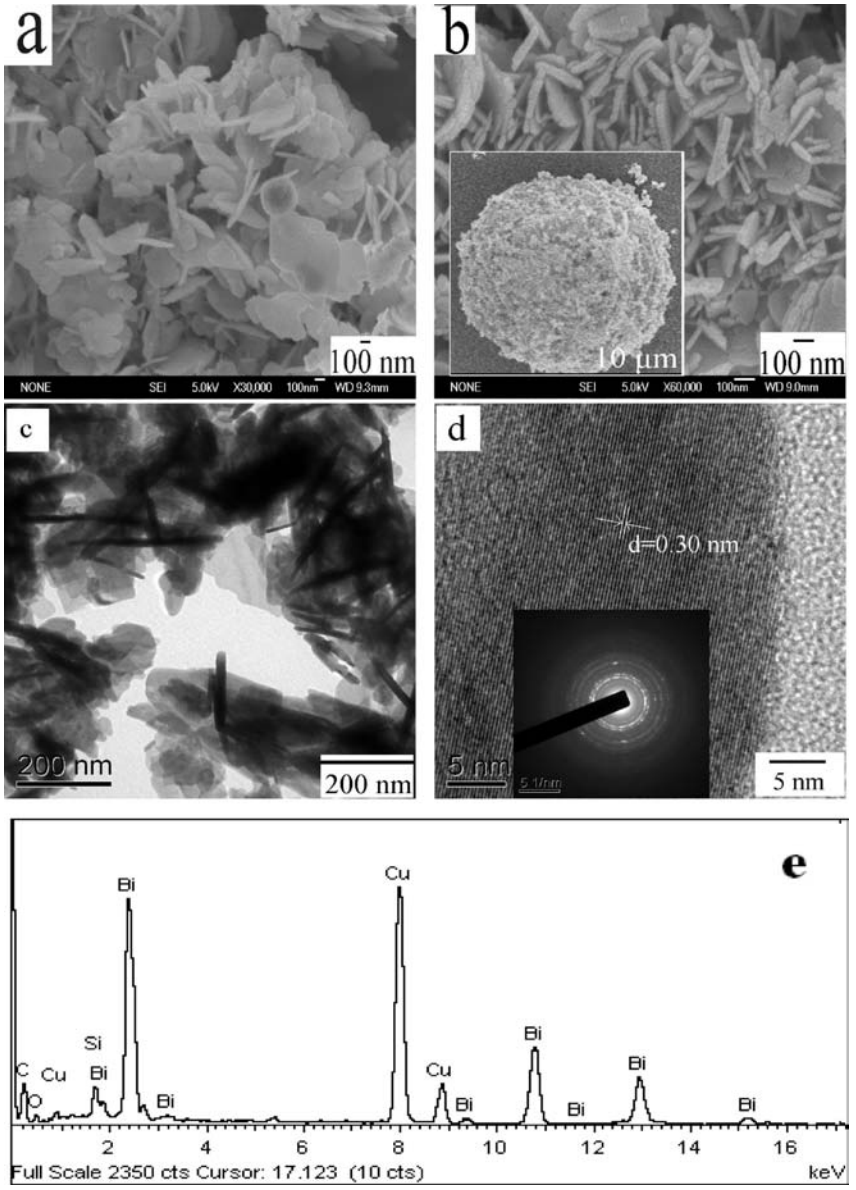

Figure 2. (a) SEM image of the sample BSO(1). (b) SEM image of the sample BSO(2) and overall morphology of the sample BSO(2) (inset). (c) TEM images of BSO(2) nanosheets. (d) HRTEM image of an individual nanosheet taken from c and SAED patterns (inset). (e) EDS pattern of the as-obtained BSO(2) nanosheets.

BSO(2). Moreover, the results of BET surface area analysis show that the BET surface areas of these two samples are 4.83 for BSO(1) and 6.44 m^2/g for BSO(2), respectively.

3.2. Morphologies of the Bi_2SiO_5 Products. The morphology and structure of the products were examined using a field emission scanning electron microscope (JSM-6700F SEM) and transmission electron microscopy (JEOL JEM-2010 EX, 200 kV) measurements. As shown in Figure 2a and b, SEM micrographs reveal that products of BSO(1) consist of a large quantity of irregular nanosheets, whereas those of BSO(2) have relatively uniform nanosheets with many biscuit-like boundaries. In addition, these nanosheets are apt to forming large microspheres (Figure 2b insert). As can be seen, the nanosheets of the sample BSO(2) are smaller and thicker than those of the sample BSO(1). A corresponding TEM image of BSO(2) nanosheets is shown in Figure 2c. The thicknesses of these nanosheets are in the range of 10−20 nm. The spacing of the lattice fringes is found to be about 0.30 nm, as shown in Figure 2d. This can be attributed to the (311) plane of the BSO crystal, which is the strongest crystallographic plane. The selected area electron diffraction pattern of the BSO(2) nanosheet is shown as the inset of Figure 2d, which reveals the well-pronounced diffraction rings, demonstrating a polycrystalline structure. The result from EDS displays that the sample contains Bi, Si, Cu, O, and C elements, as shown in Figure 2e. The elements of Cu and C are generated from the supporting carbon-coated copper meshes.

3.3. UV−Vis Diffuse Reflectance Absorption Spectra of Bi_2SiO_5 Products. Figure 3 shows the room-temperature UV−vis diffuse reflectance spectra of two samples with different Si sources, which were recorded on a UV−vis spectrophotometer. The wavelength at the absorption edge, λ, is determined as the intercept on the wavelength

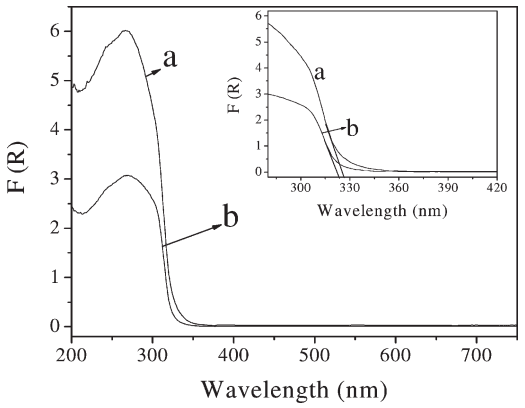

Figure 3. UV−vis diffuse reflectance of as-prepared BSO samples: (a) BSO(1) and (b) BSO(2).

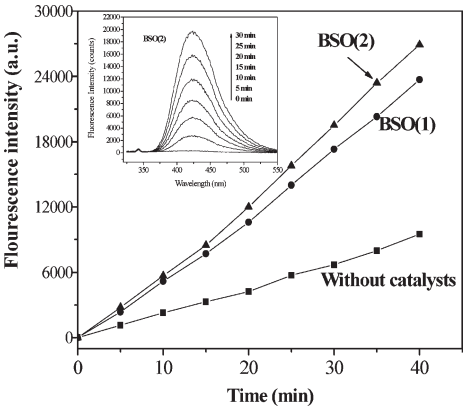

Figure 4. Plots of the induced fluorescence intensity at 426 nm against irradiation time for terephthalic acid on the sample BSO. Inset: Fluorescence spectral changes observed during illumination of BSO(2) in a solution of terephthalic acid (excitation at 312 nm, emission at 426 nm).

axis for a tangent line drawn on absorption spectra. The absorption for the two samples locates at ca. 328 nm (Figure 3a) and 324 nm (Figure 3b), respectively. The band gap energies (E_g) calculated on the basis of the corresponding absorption edges are 3.78 and 3.83 eV. The blue shift in the band gap for the sample BSO(2), using Na_2SiO_3 a as Si source, may be attributed to quantum confinement effects because of the small size regime.[12] As can be expected on the basis of the absorption spectra, the samples are white in color.

3.4. •OH-Trapping Photoluminescence Spectra. In the photocatalytic process, the photogenerated holes can react with adsorbed water to form •OH radicals, which are the major active oxidation species in the decomposition of organic pollutants. Terephthalic acid was used to readily react with •OH to form highly fluorescent products and 2-hydroxyterephthalic acid, which can be detected by fluorescence spectroscopy (excitation wavelength, 312 nm; fluorescence peak, 426 nm).[13] The amount of •OH radical could be estimated from the fluorescence intensity. The inset of Figure 4 shows the •OH-trapping photoluminescence spectra of sample BSO(2) in a terephthalic acid solution at room temperature under UV-light irradiation. This implies that fluorescent products formed during the photocatalytic process, which is due to the specific reaction between •OH and terephthalic acid. The fluorescence intensity at 426 nm increases when UV light is irradiated continuously. The stronger fluorescence intensity means that more •OH is produced. As the relation between fluorescence intensity and irradiation time is linear, the formed •OH is proportional to irradiation time. The generated rate of •OH can be calculated by the slope of straight lines in Figure 4. It exhibits that the linear slope of the change in fluorescence intensity for sample BSO(2) is steeper than that for sample BSO(1), suggesting that a greater formation rate of •OH radicals occured over sample BSO(2). The greater the formation rate of •OH radicals is, the higher the separation efficiency of electron−hole pairs is achieved. Therefore, higher photocatalytic activity can be predicted.

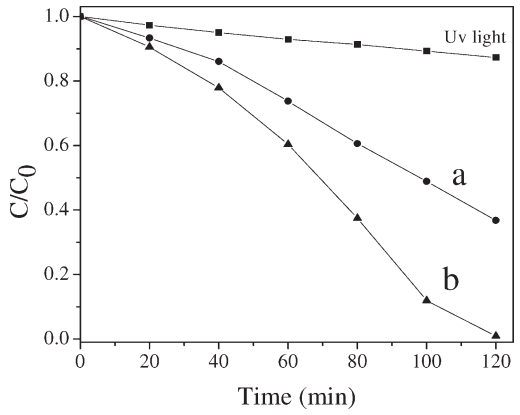

Figure 5. Concentration changes of salicylic acid at 297 nm as a function of light irradiation time in the presence of photocatalysts: (a) BSO(1) and (b) BSO(2).

3.5. Photocatalytic Properties of the Bi_2SiO_5 Products. The photocatalytic activities of the samples were first evaluated by the degradation of salicylic acid. Figure 5 displays the concentration changes of salicylic acid at 297 nm as a function of irradiation time during the degradation process in aqueous solution in the presence of BSO samples. After UV irradiation for 120 min, about 63% (Figure 5a) of the salicylic acid is degraded in the case of the sample BSO(1), while in the case of the sample BSO-(2), it is interesting to note that 99% of the salicylic acid in the solution is decomposed (Figure 5b). As is well-known, the photocatalytic activity of a catalyst for the degradation of pollutants is related to its band gap energy owing to its nanosized structures and high surface areas.[14] In our experiment, it is easy to recognize that the effective surface area of BSO(2) is larger than that of BSO(1). Thus, the higher photocatalytic activity of the BSO(2) sample can be ascribed to its small size, which leads to an increase both in the band gap energy and in the surface area.[15] In addition, the change in the morphology also affects the photocatalytic activity of BSO. The high photocatalytic activity of BSO(2) is probably due to the existence of many biscuit-like boundaries, which functions as a separation between the photogenerated

(12) Zhu, J. W.; Chen, H. Q.; Liu, H. B.; Yang, X. J.; Lu, L. D.; Wang, X. *Mater. Sci. Eng., A* **2004**, *384*, 172.
(13) Bi, J. et al. *Appl. Catal., B.* **2009**, DOI: 10.1016/j.apcatb.2009.05.016.
(14) (a) Jang, E. S.; Won, J. H.; Hwang, S. J.; Choy, J. H. *Adv. Mater.* **2006**, *18*, 3309. (b) Hoffmann, M. R.; Martin, S. T.; Choi, W.; Bahnemann, D. W. *Chem. Rev.* **1995**, *95*, 69.
(15) Yang, J. L.; An, S. J.; Park, W. I.; Yi, G. C.; Choi, W. Y. *Adv. Mater.* **2004**, *16*, 1661.

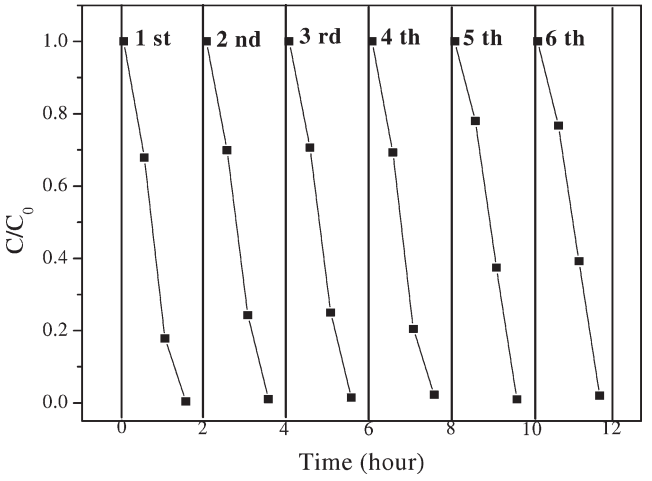

Figure 6. The lifetime for photodegradation of salicylic acid on sample BSO(2).

electron−hole pairs, therefore forming more •OH radicals, confirmed by •OH-trapping photoluminescence spectra, and facilitates the degradation of salicylic acid to some degree. To investigate the photoactivity of the Bi_2SiO_5 sample toward other organic compounds, gaseous benzene was employed. Both of the two samples have a similar benzene conversion ratio of about 5%. However, for BSO(1), only a small amount of CO_2 (ca. 25 ppm) is produced, but 35 ppm of CO_2 can be detected for the sample BSO(2). The order of the photocatalytic activities of two samples is consistent for either the degradation of salicylic acid in aqueous solution or the removal of benzene in gas.

The stability of a photocatalyst is very important for its application. Herein, the stability of Bi_2SiO_5 was investigated via the decomposition of salicylic acid. The lifetime for Bi_2SiO_5 is shown in Figure 6. The results reveal that the sample does not exhibit an obvious loss of activity.

In the present work, the BET specific surface areas of the as-prepared BSO samples are only 4−6 m^2/g, which are much lower than that of Degussa P25 (50 m^2/g). The photocatalytic performances of our products are somewhat poorer than that of P25, as expected. Therefore, it is expected to exploit new method in the preparation process to improve the specific surface areas.

4. Conclusions

In summary, a template-free hydrothermal process has been developed in preparing orthorhombic two-dimensional (2D) Bi_2SiO_5 nanosheets for the first time. The UV−vis absorption spectra show that the as-prepared nanomaterials have a strong absorption edge in UV light and that their band gaps are somewhat relevant to the size and morphology. Relatively uniform Bi_2SiO_5 nanosheets have been obtained by using Na_2SiO_3 as a Si source. Photocatalytic evaluations via the decomposition of salicylic acid and benzene under UV-light irradiation reveal that samples obtained by different Si sources exhibit different photocatalytic performances. The highest photocatalytic activity is obtained by the sample BSO(2) because of an increase both in the band gap energy and in the surface areas of uniform nanosheet structures. Further work is under way to study the ferroelectric and dielectric properties of BSO nanosheets, as well as the possibility of synthesizing other nanostructrues.

Acknowledgment. The authors are grateful for financial support by the National Natural Science Foundation of China (20777011, 20537010, and 20677009), National Key Basic Research Program of China (973 Program: 2007CB613306 and 2008CB617507), and Program for Changjiang Scholars and Innovative Research Team in University (PCSIRT0818).